

Deformation effects on sub-barrier fusion cross sections in $^{16}\text{O} + ^{174,176}\text{Yb}$

Tapan Rajbongshi,¹ K. Kalita,^{1,*} S. Nath,² J. Gehlot,² Tathagata Banerjee,² Ish Mukul,³ R. Dubey,² N. Madhavan,² C. J. Lin,⁴ A. Shamlath,⁵ P. V. Laveen,⁵ M. Shareef,⁵ Neeraj Kumar,⁶ P. Jisha,⁷ and P. Sharma⁸

¹Department of Physics, Gauhati University, Guwahati 781014, India

²Nuclear Physics Group, Inter University Accelerator Centre, Aruna Asaf Ali Marg, New Delhi 110067, India

³Department of Particle Physics and Astrophysics, Weizmann Institute of Science, Rehovot 76100, Israel

⁴China Institute of Atomic Energy, P. O. Box 275(10), Beijing 102413, People's Republic of China

⁵Department of Physics, School of Mathematical and Physical Sciences, Central University of Kerala, Kasaragod 671328, India

⁶Department of Physics and Astrophysics, University of Delhi, Delhi 110007, India

⁷Department of Physics, University of Calicut, Calicut 673635, India

⁸Department of Physics, Panjab University, Chandigarh 160014, India

(Received 3 February 2016; revised manuscript received 5 April 2016; published 25 May 2016)

Background: Couplings with various reaction channels are known to enhance sub-barrier fusion cross sections by several orders in magnitude. However, a few open questions still remain. For example, the influence of higher order static deformations on sub-barrier fusion cross sections is yet to be comprehensively understood.

Purpose: We study the role of hexadecapole nuclear deformation effect on sub-barrier fusion cross sections. Also, this work aims to extract hexadecapole deformation (β_4) in nuclei in the lanthanide region.

Method: The evaporation residue (ER) excitation functions for $^{16}\text{O} + ^{174,176}\text{Yb}$ were measured at laboratory beam energies (E_{lab}) in the range of 64.6–103.6 MeV. Measurements were carried out by employing the recoil mass spectrometer Heavy Ion Reaction Analyzer (HIRA) at IUAC, New Delhi. Fusion barrier distributions (BDs) were extracted from data. Results from the experiment were subjected to coupled-channels analysis, in which β_4 was varied as a free parameter.

Results: Experimental fusion cross sections at energies below the barrier expectedly showed strong enhancement compared to the predictions from the one-dimensional barrier penetration model. Data were satisfactorily reproduced after inclusion of negative β_4 for both the targets in the coupled-channels calculation.

Conclusions: The significant role of hexadecapole deformation was observed in the sub-barrier fusion of $^{16}\text{O} + ^{174,176}\text{Yb}$. The proposed value of β_4 reproduced the measured fusion excitation function reasonably well. The BDs from these data were also extracted but no definitive conclusions could be drawn from them.

DOI: [10.1103/PhysRevC.93.054622](https://doi.org/10.1103/PhysRevC.93.054622)

I. INTRODUCTION

Heavy ion-induced fusion reactions around the Coulomb barrier have been pursued quite intensely for the past few decades [1–4]. Fusion cross sections are found to be enhanced, in some cases by several orders of magnitude, over the prediction from the one-dimensional barrier penetration model near and below the Coulomb barrier [5,6]. The coupling of internal degrees of freedom such as transfer of valence neutrons, neck formation, zero point motion, and static deformation have been considered in order to explain observed enhancements of the fusion cross sections. The coupling with intrinsic degrees of freedom has an effect of changing the height of the barrier. Barriers lower than the one-dimensional Coulomb barrier are then responsible for the enhancement of fusion cross sections.

Deformation of one or both the reaction partners is known to enhance sub-barrier fusion cross sections [7–10]. The extent to which a particular degree of freedom (e.g., quadrupole or hexadecapole deformation) contributes to the sub-barrier fusion enhancement independently can be estimated by calculating the asymptotic energy shift [11] associated with that particular degree of freedom [12–14]. Besides, the idea that a positive β_4 could enhance sub-barrier fusion cross sections

more, in comparison to what a negative β_4 does, was put forward for the reaction $^{16}\text{O} + ^{186}\text{W}$ [15]. On the other hand, due to negative hexadecapole deformations, enhancements of sub-barrier fusion cross sections have been measured for the reactions ^{16}O on $^{176,180}\text{Hf}$ and $^{182,184,186}\text{W}$ by Leigh *et al.* [16]. Also the same conclusion was drawn theoretically for the $^{16}\text{O} + ^{184}\text{W}$ system [17].

The barrier distributions (BDs) are known to be highly sensitive to higher order nuclear deformations. The experimental BDs can be obtained from the fusion cross sections [2,18] as well as from quasielastic scattering data [19,20]. The shapes of the experimental BDs extracted from the fusion excitation functions [9] for $^{16}\text{O} + ^{154}\text{Sm}$ and $^{16}\text{O} + ^{186}\text{W}$ reveal that the role of positive and negative β_4 is evident in the qualitative differences between the two BDs.

We performed an experiment to measure ER excitation functions for the systems $^{16}\text{O} + ^{174,176}\text{Yb}$ forming compound nuclei (CN) $^{190,192}\text{Pt}$ near and below the Coulomb barrier. Since ^{16}O is a doubly magic spherical nucleus, effects of nuclear shapes on fusion cross sections are expected to be solely due to target nuclei. We investigated the role of β_4 in reproducing fusion data with the help of coupled-channels (CC) calculations. The experimental details are described in Sec. II while analysis of data and results are presented in Sec. III. We summarize our work and conclude in Sec. IV.

*ku_kalita@yahoo.com

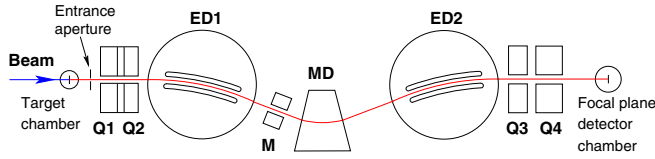


FIG. 1. Schematic of the recoil mass spectrometer HIRA [21]. Q, ED, M, and MD stand for magnetic quadrupole, electrostatic dipole, magnetic multipole, and magnetic dipole, respectively.

II. THE EXPERIMENT

The experiment was performed at the 15 UD Pelletron accelerator facility of IUAC. A pulsed beam of ^{16}O with a pulse separation of $4\ \mu\text{s}$ was incident upon isotopically enriched ^{174}Yb (99.99%) and ^{176}Yb (96.63%) targets of thickness $125\ \mu\text{g}/\text{cm}^2$ and $170\ \mu\text{g}/\text{cm}^2$, respectively, on $25\ \mu\text{g}/\text{cm}^2$ $^{\text{nat}}\text{C}$ backing. Evaporation residue (ER) excitation functions were measured at laboratory beam energies (E_{lab}) of 64.6–79.6 MeV, in steps of 1 MeV, and 81.6–103.6 MeV, in steps of 2 MeV (at the center of the targets). ERs were separated from overwhelmingly dominant background events using the schematic of recoil mass spectrometer Heavy Ion Reaction Analyzer (HIRA) [21] in Fig. 1.

Two silicon detectors were placed inside the target chamber at $\pm 15.5^\circ$ with respect to the beam direction in the horizontal plane to record Rutherford-scattered beam particles for absolute normalization of ER cross sections. To reset charge states of the ERs, a $30\ \mu\text{g}/\text{cm}^2$ thick $^{\text{nat}}\text{C}$ foil was placed 10 cm downstream from the target. A multiwire proportional counter (MWPC), with an active area of $150\ \text{mm} \times 50\ \text{mm}$, was placed at the focal plane of the HIRA to detect the ERs. A very thin ($0.5\ \mu\text{m}$) mylar foil was used as the entrance window of the MWPC, which separated the gas volume (3 mbar isobutane) of the MWPC from the vacuum inside the HIRA. Time of flight (TOF) of the ERs, over the distance from the target to the anode of the MWPC, was also recorded. The HIRA was operated with 10 msr acceptance and at 0° with respect to the beam direction.

IUAC's in-house data acquisition software CANDLE [22] was employed to record list-mode data, whereas analysis was performed with the aid of CANDLE and ROOT [23].

III. DATA ANALYSIS AND RESULTS

The total ER cross section is given by

$$\sigma_{\text{ER}} = \frac{Y_{\text{ER}}}{Y_{\text{norm}}} \left(\frac{d\sigma}{d\Omega} \right)_{\text{Ruth}} \Omega_{\text{norm}} \frac{1}{\bar{\epsilon}_{\text{HIRA}}} \quad (1)$$

where Y_{ER} is the ER yield at the focal plane of the HIRA, Y_{norm} is the number of Rutherford-scattered projectiles recorded by any of the normalization detectors, Ω_{norm} is the solid angle subtended by any of the normalization detectors, and $\left(\frac{d\sigma}{d\Omega} \right)_{\text{Ruth}}$ is the differential Rutherford scattering cross section in the laboratory frame of reference. $\bar{\epsilon}_{\text{HIRA}}$ is the average ER transmission efficiency through the HIRA.

There were two major challenges in extracting σ_{ER} from the experiment: (a) estimation of $\bar{\epsilon}_{\text{HIRA}}$ and (b) unambiguous identification of ERs at the focal plane of the HIRA.

The transmission efficiency (ϵ_{HIRA}) is a complex function of several reaction-specific and instrument-specific parameters [24]. It is defined as the ratio of number of ERs reaching the focal plane to the total number of ERs emerging from the target. As measuring ϵ_{HIRA} for each exit channel at each E_{lab} was not practicable, we relied on the semimicroscopic Monte Carlo code TERS [25] to calculate ϵ_{HIRA} . We further followed the formalism presented in Ref. [24] to estimate $\bar{\epsilon}_{\text{HIRA}}$, the transmission efficiency of HIRA averaged over all dominant exit channels at a given E_{lab} . The relative population of different ER channels in the reactions $^{16}\text{O} + ^{174,176}\text{Yb}$ was estimated by the statistical model code PACE3 [26].

The next major challenge was to identify ER events unambiguously from background events. Simultaneous measurement of energy loss (ΔE) and TOF of the ERs usually results in clear separation of ERs from projectile-like background events. Scatter plots of ΔE versus TOF at several E_{lab} for the reaction $^{16}\text{O} + ^{174}\text{Yb}$ are shown in Fig. 2. One can notice that the strategy of identifying ERs based on ΔE and TOF works rather well up to $\frac{E_{\text{c.m.}}}{V_{\text{B}}} \approx 1$. With decreasing E_{lab} , unambiguous identification of ERs becomes increasingly difficult. This is because yield of ERs decreases (as σ_{ER} falls exponentially) and yield of background events increases significantly (with increasing Rutherford cross section) overlapping with ER events in the ΔE versus TOF plots.

One must note here that measured TOF was not absolute, as the time delays between the start (arrival of a particle at the focal plane) and stop (250 kHz rf) pulses were often adjusted because of practical reasons during the experiment. Hence an absolute and global calibration of the TOF spectra spanning the entire range of E_{lab} was not possible. We scrutinized those ΔE versus TOF plots from both the reactions, which showed clear separation between ER events and background events, to look for any underlying correlation between the two groups of events. We further projected the events in each spectrum on the TOF axis and noted the centroid and FWHM (wherever the peak could be fitted with a Gaussian) of each group of events. We finally made the following empirical observations from the projected spectra: (a) the difference between the centroids increases linearly with decreasing E_{lab} , (b) the FWHM of the ER group increases linearly with decreasing E_{lab} , and (c) the peak of the ER group is approximately symmetric about the centroid. The probable centroid and FWHM of the ER group of events at $\frac{E_{\text{c.m.}}}{V_{\text{B}}} < 1$, where ERs are not clearly separated from background, were then determined by least-squares linear fit and extrapolation. The rectangular gates to obtain ER yields, as shown in Fig. 2, were then positioned by applying observations (a) and (b). Each rectangular gate in Fig. 2 is divided into two equal halves by a dotted line. Observation (c) ensured that ER counts in both halves are nearly equal. This characteristic of the plots helped reduce background further. We observed presence of background events in the lower half of the rectangular gate at a few E_{lab} below the barrier. This was revealed by the fact that counts in the upper half of the gate were much lower in comparison with those in the lower half of the gate. We further confirmed this observation by carrying out measurement with a blank target.

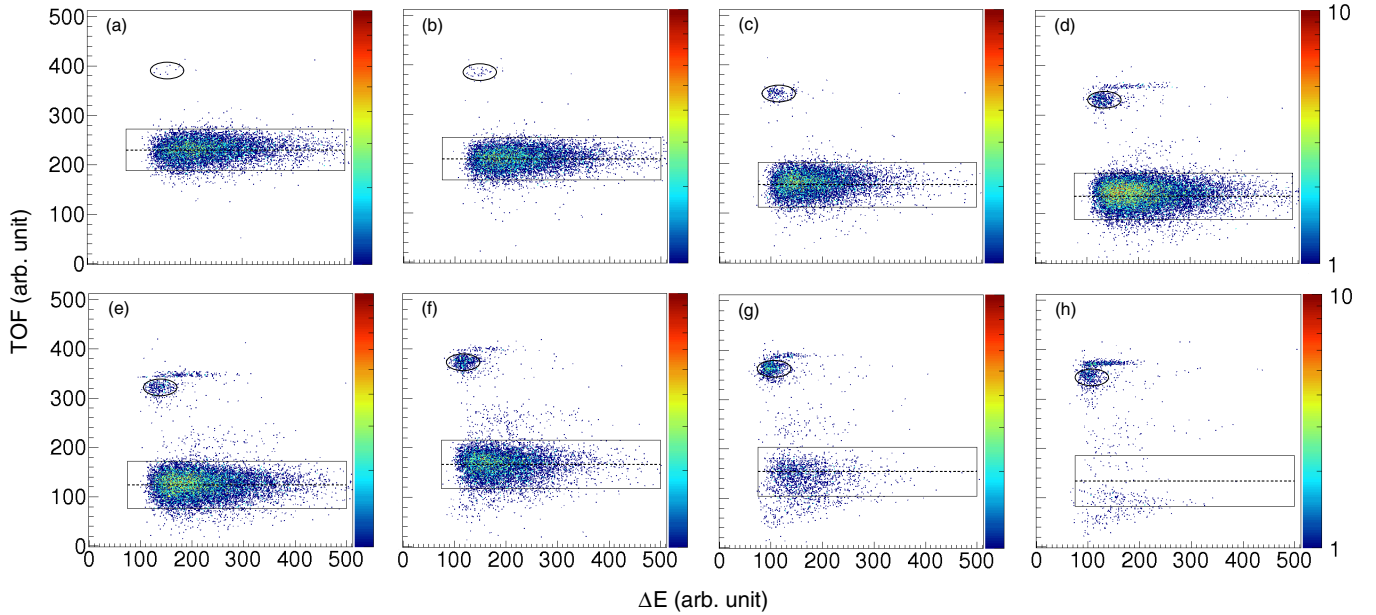


FIG. 2. Scatter plots between ΔE and TOF of the events recorded at the focal plane of HIRA for $^{16}\text{O} + ^{174}\text{Yb}$ at various E_{lab} : (a) 101.6 MeV ($\frac{E_{\text{c.m.}}}{V_B} \approx 1.40$), (b) 95.6 MeV ($\frac{E_{\text{c.m.}}}{V_B} \approx 1.30$), (c) 87.6 MeV ($\frac{E_{\text{c.m.}}}{V_B} \approx 1.20$), (d) 79.6 MeV ($\frac{E_{\text{c.m.}}}{V_B} \approx 1.10$), (e) 76.6 MeV ($\frac{E_{\text{c.m.}}}{V_B} \approx 1.05$), (f) 72.6 MeV ($\frac{E_{\text{c.m.}}}{V_B} \approx 1.00$), (g) 69.7 MeV ($\frac{E_{\text{c.m.}}}{V_B} \approx 0.95$), and (h) 65.7 MeV ($\frac{E_{\text{c.m.}}}{V_B} \approx 0.90$). Here $E_{\text{c.m.}}$ and V_B are the projectile energy and the Coulomb barrier, respectively, in the center-of-mass (c.m.) frame of reference. ERs are seen within the rectangular gate in each panel. Projectile-like background events, one group of which is encircled within an elliptical gate, are seen at the top-left corner of each panel. See text for details.

Figure 3(a) shows ΔE versus TOF plot for the reaction $^{16}\text{O} + ^{176}\text{Yb}$ at $E_{\text{lab}} = 66.6$ MeV. Figure 3(b) shows a similar plot with data taken with a blank target, keeping all other experimental conditions unchanged. One can notice that the lower half of the rectangular gate in Fig. 3(b) contain events even though ERs were not produced in this case. Whenever we noted a large difference between ER counts in the two halves of the rectangular gate, indicating presence of background, we considered double the count in the upper half of the gate to be the ER yield.

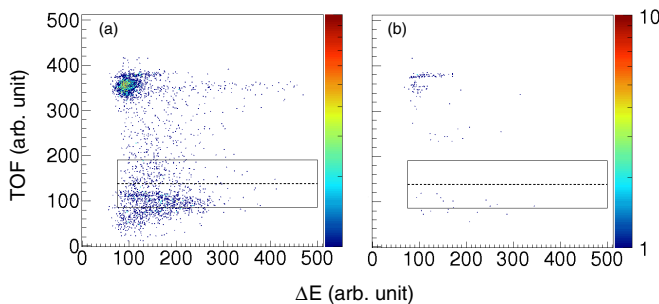


FIG. 3. Scatter plots between ΔE and TOF of the events recorded at the focal plane of HIRA at $E_{\text{lab}} = 66.6$ MeV: (a) with ^{176}Yb as the target and (b) with a blank target frame in place. Beam current and HIRA settings were kept the same during both the runs. The background data, with no target material in place, were collected for a shorter duration, namely, \sim one-eighth the duration of data collection with the ^{176}Yb target. See text for details.

Yield of ER and $\bar{\epsilon}_{\text{HIRA}}$, thus obtained, were fed into Eq. (1) to determine σ_{ER} . Excitation functions for the reactions $^{16}\text{O} + ^{174}\text{Yb}$ and $^{16}\text{O} + ^{176}\text{Yb}$ are shown in Figs. 4 and 5, respectively. We must point out here that isotopic or other impurities with nearby mass numbers in the target may affect deduced cross sections. The excitation functions show an upward trend at the two lowest E_{lab} for both reactions, which might be caused by the presence of impurities in the targets. This feature is particularly accentuated in data with the ^{176}Yb target, which is relatively of lesser purity (96.63%).

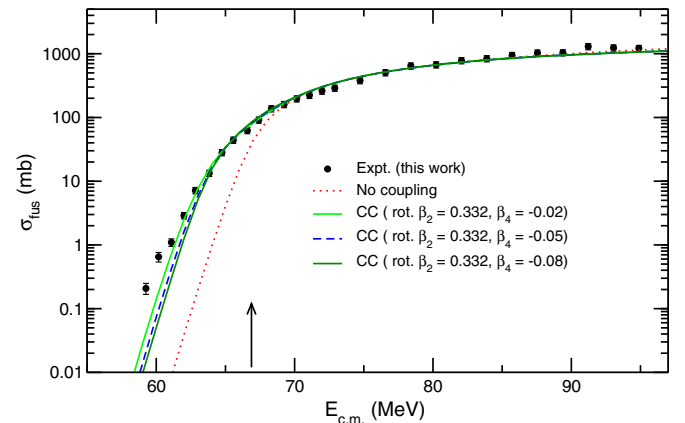


FIG. 4. The experimental fusion excitation functions for $^{16}\text{O} + ^{174}\text{Yb}$ along with results from CC calculations using CCFULL. The arrow indicates position of the Coulomb barrier.

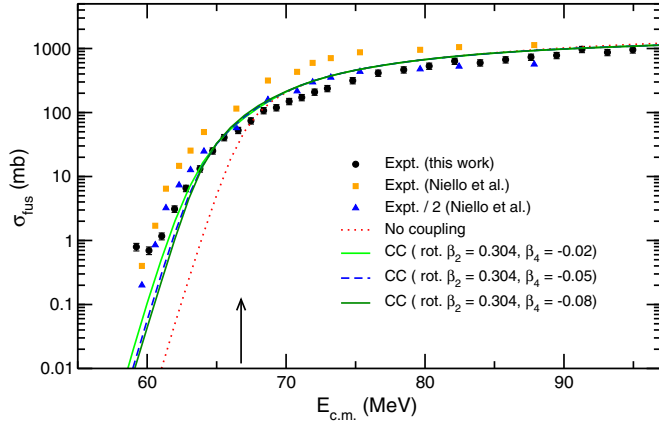


FIG. 5. The experimental fusion excitation functions for $^{16}\text{O} + ^{176}\text{Yb}$ along with results from CC calculations using CCFULL. Data from Ref. [7] are also shown. The arrow indicates position of the Coulomb barrier.

An excited CN in the lighter mass region decays by emission of γ photons and evaporation of neutrons and light charged particles, yielding a cold ER. As the CN becomes heavier, it decays by fission (CNF) besides the ER channels. In the still heavier mass regions, fusion probability (P_{CN}) itself starts deviating from unity as non-CN fission (NCNF) channels open up. In a recent work [27], a systematic study of fusion probability in heavy nuclei, at energies above the Coulomb barrier, was reported covering the mass region 170 to 220, in which the authors pointed out approximate boundaries from where NCNF appears to become significant. According to the prescriptions suggested in Ref. [27], the present reactions are expected to proceed via CN formation alone after capture inside the potential barrier. Also, population of CNF channels in the present reactions in the studied range of E_{lab} is not significant [28]. Because of these reasons, the measured ER excitation function was taken as the fusion excitation function for both reactions in the present work.

The CC calculations were performed by using the code CCFULL [29]. The deformation parameters and excitation energies of the participating nuclei are listed in Table I. The Woods-Saxon parametrization of the Akyüz-Winther potential [33] was used in CCFULL. The nuclear potential was approximated by using the parameters $V_0 = 63.53$ MeV, $r_0 = 1.19$ fm, and $a = 0.66$ fm for the $^{16}\text{O} + ^{174}\text{Yb}$ reaction and $V_0 = 63.63$ MeV, $r_0 = 1.19$ fm, and $a = 0.66$ fm for the $^{16}\text{O} + ^{176}\text{Yb}$ reaction in CCFULL. There is a slight change in the radius parameter (r_0) and diffuseness parameter (a) of

TABLE I. The deformation parameters [30,31] and excitation energies [30,32] of different nuclei used in the CC calculations.

Nucleus	^{16}O	^{174}Yb	^{176}Yb
E_{2+} (MeV)		0.076	0.082
β_2 (rot.)		0.332	0.304
E_{3-} (MeV)	6.13	1.381	1.491
β_3 (vib.)	0.733	0.051	0.024

the real nuclear potential to fit the experimental data. Hagino *et al.* [6] mentioned that energy of the 3^- state of ^{16}O is very high compared to the barrier curvature. Without affecting the structure of the BD it only produces an adiabatic potential renormalization. Therefore, this coupling was not considered. Rotational as well as vibrational couplings of both the targets were treated to all orders in the CC calculation. Due to the minor effects in the lower energy region, the vibrational couplings were not shown in CC calculation. We varied the value of β_4 to fit the experimental data, keeping all other parameters fixed. The fusion excitation functions and results of the CC calculations with different β_4 are shown in Figs. 4 and 5, respectively.

The red dotted line in the figures is the prediction from the one-dimensional barrier penetration model, which expectedly underestimates data. The results of CC calculation have been plotted in Figs. 4 and 5 respectively with a fixed value of β_2 and varying β_4 as -0.020 (solid light-green line), -0.050 (dashed blue line) and -0.080 (solid dark-green line) to explain the fusion excitation function. Considering coupling to rotational $\beta_2 = 0.332$, $\beta_4 = -0.020$ for ^{174}Yb and $\beta_2 = 0.304$, $\beta_4 = -0.020$ for ^{176}Yb target nuclei gave satisfactory fits to data from well above to the sub-barrier region. But none of these values (-0.020 to -0.080) exactly fit the sub-barrier fusion data. We also investigated the sensibility of the CC calculations with slight change in above β_4 range, but no significant improvement was obtained. Therefore, we proposed the hexadecapole parameter $\beta_4 = -0.020$, which gave at least satisfactory fit to sub-barrier fusion data for both the systems. This extracted value may bring about an uncertainty due to the noninclusion of additional couplings like vibrational, transfer channels, etc., in the CC calculation. The extracted new value of β_4 for $^{174,176}\text{Yb}$ agreed reasonably well with available results as shown in Table II. The fusion cross sections measured by Niello *et al.* [7] for the system $^{16}\text{O} + ^{176}\text{Yb}$ are also shown (solid squares) in Fig. 5, which disagree with both the present data and the calculated cross sections below as well as above the barrier. Matching of the data of Niello *et al.* data with the present results demands an arbitrary division of the former by a factor of 2 (solid triangle as shown in Fig. 5).

We next extracted BD from fusion excitation functions using the point difference formula. The second derivative of $E\sigma$ with respect to energy [2] give rise to BD. This expression at energy $(E_1 + 2E_2 + E_3)/4$ is given by

$$\frac{d^2(\sigma E)}{dE^2} = 2 \left[\frac{(E\sigma)_3 - (E\sigma)_2}{E_3 - E_2} - \frac{(E\sigma)_2 - (E\sigma)_1}{E_2 - E_1} \right] \frac{1}{E_3 - E_1}, \quad (2)$$

where $(E\sigma)_i$ are evaluated at energies E_i . For data with $\Delta E = (E_2 - E_1) = (E_3 - E_2)$, i.e., equal energy steps,

$$\frac{d^2(\sigma E)}{dE^2} = \frac{(E\sigma)_3 - 2(E\sigma)_2 + (E\sigma)_1}{\Delta E^2}. \quad (3)$$

The statistical error δ associated with the second derivative at energy E was calculated using the equation

$$\delta = \left(\frac{E}{\Delta E^2} \right) [(\delta\sigma_{\text{fus}})_1^2 + 4(\delta\sigma_{\text{fus}})_2^2 + (\delta\sigma_{\text{fus}})_3^2]^{\frac{1}{2}}, \quad (4)$$

TABLE II. Measured/calculated hexadecapole deformation of $^{174,176}\text{Yb}$.

Nucleus	β_4	Method	Ref.	Nucleus	β_4	Method	Ref.
^{174}Yb	-0.040, -0.052	α scattering	[31,35]	^{176}Yb	-0.045, -0.059, -0.046	α scattering	[31,35]
	-0.041, -0.030	α scattering	[31,35]		0.012, 0.011	Coulomb excitation	[36]
	-0.007, -0.007	Coulomb excitation	[36]		-0.037	theoretical	[37]
	-0.024	theoretical	[37]		-0.050	theoretical	[38]
	-0.050	theoretical	[38]		-0.032	theoretical	[39,40]
	-0.021	theoretical	[39,40]		-0.054, -0.054, -0.0875	electron scattering	[41]
	-0.053	quasielastic	[20]		-0.071	theoretical	[42]
	-0.059	theoretical	[42]		-0.350	α scattering	[43]
-0.020	fusion excitation	[this work]	-0.020	fusion excitation	[this work]		

where $(\delta\sigma_{\text{fus}})$ are the absolute errors in the cross sections. A ΔE of 2 MeV (laboratory) was used for this work to obtain the second derivative.

BDs obtained from the fusion excitation functions and CC calculations for the reactions $^{16}\text{O} + ^{174}\text{Yb}$ and $^{16}\text{O} + ^{176}\text{Yb}$ are shown in Figs. 6 and 7, respectively. In CC calculations, we included the coupling to rotational β_2, β_4 of target nuclei. It can be seen that the CC calculation with $\beta_4 = -0.020$ gives good reproduction for the barrier distribution at lower energies. The BD can have a wide range that would be expected classically, due to the random orientation of the deformed target nuclei. The BDs are reasonably well defined at low energies, but around the peak of the distribution and near the average barrier the uncertainties were larger than the measured values. As seen in Figs. 6 and 7, the BDs show a broad single peak with large fluctuations at higher energies. It is quite obvious that more precise data than what we had at hand would be required to determine proper shape of the BD. The thickness of targets in the present work was clearly not suitable for measurement of BD. Consequently, it was not possible to draw proper conclusions from BDs independently. The derived BDs were not useful to determine the value of β_4 .

We must note here that experimental determination of β_4 is difficult. Also, results are highly model dependent [20,34]. There are reported disagreements between measurements and between measured and calculated values of β_4 for a given

nucleus. Table II summarizes β_4 for $^{174,176}\text{Yb}$, determined either from data or calculation.

IV. SUMMARY AND CONCLUSIONS

We measured the ER excitation functions around the Coulomb barrier for the reactions $^{16}\text{O} + ^{174,176}\text{Yb}$ using the recoil mass spectrometer HIRA. Utmost caution was exercised in identifying ERs, particularly at the lowest energies, so that those are not contaminated with more abundant background events. Since presence of CNF and NCNF in these reactions are expected to be insignificant, measured ER excitation functions were taken as the fusion excitation functions. CC calculations were performed with the code CCFULL to interpret data. Fusion barrier distributions were also extracted from the cross sections. Coupling to rotational β_2, β_4 (-0.020 for ^{174}Yb and ^{176}Yb) of the target nuclei explained the fusion excitation functions satisfactorily. Our experimental results suggested a new hexadecapole parameter (β_4) value of -0.020 for the present systems. Experimentally determined β_4 are susceptible to systematic uncertainties and also heavily dependent on the model used in a particular work. Thus, more precise measurements in this mass region using different experimental techniques are called for to achieve convergence of the results and overcome dependence on models.

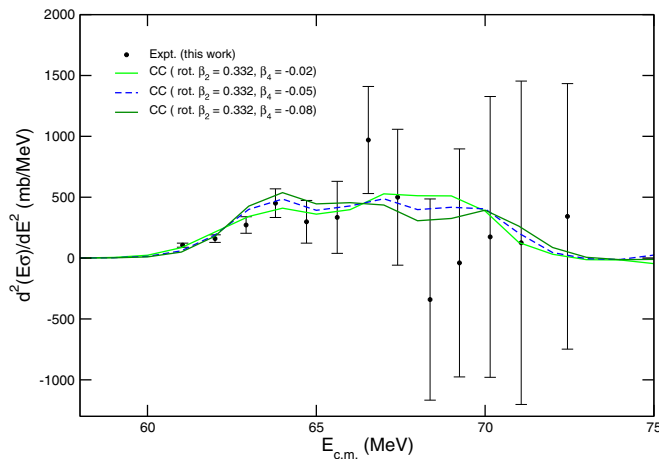


FIG. 6. Experimentally extracted BD for $^{16}\text{O} + ^{174}\text{Yb}$. The results from CC calculation are shown as indicated.

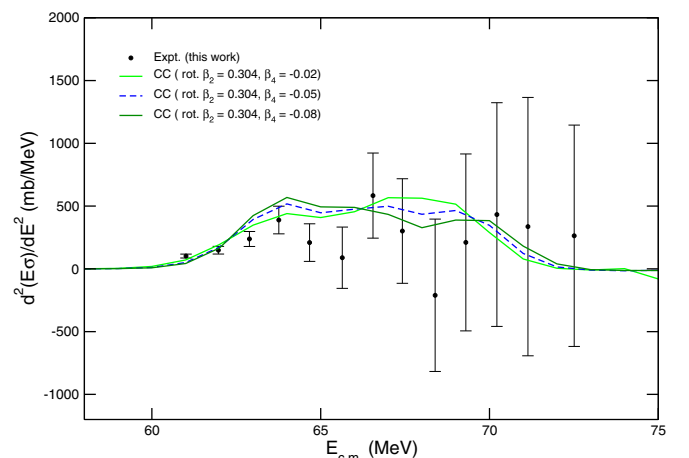


FIG. 7. The same as Fig. 6 but for $^{16}\text{O} + ^{176}\text{Yb}$.

ACKNOWLEDGMENTS

The authors are thankful to the Pelletron staff of IUAC for providing pulsed beams of requisite quality throughout the experiment. Support received from the target and the

data support laboratories of IUAC is highly appreciated. K.K. would like to thank Prof. K. Hagino for useful discussions. T.R. acknowledges IUAC, New Delhi, India for financial support (IUAC/XIII.7/UFR/52314) to carry out this work.

-
- [1] A. B. Balantekin and N. Takigawa, *Rev. Mod. Phys.* **70**, 77 (1998).
- [2] M. Dasgupta, D. J. Hinde, N. Rowley, and A. M. Stefanini, *Annu. Rev. Nucl. Part. Sci.* **48**, 401 (1998).
- [3] K. Hagino and N. Takigawa, *Prog. Theor. Phys.* **128**, 1061 (2012).
- [4] B. B. Back, H. Esbensen, C. L. Jiang, and K. E. Rehm, *Rev. Mod. Phys.* **86**, 317 (2014).
- [5] J. D. Bierman, P. Chan, J. F. Liang, M. P. Kelly, A. A. Sonzogni, and R. Vandenbosch, *Phys. Rev. Lett.* **76**, 1587 (1996).
- [6] K. Hagino, N. Takigawa, M. Dasgupta, D. J. Hinde, and J. R. Leigh, *Phys. Rev. Lett.* **79**, 2014 (1997).
- [7] J. O. Fernández Niello *et al.*, *Phys. Rev. C* **43**, 2303 (1991).
- [8] J. O. Fernández-Niello and C. H. Dasso, *Phys. Rev. C* **39**, 2069 (1989).
- [9] J. R. Leigh, M. Dasgupta, D. J. Hinde, J. C. Mein, C. R. Morton, R. C. Lemmon, J. P. Lestone, J. O. Newton, H. Timmers, J. X. Wei, and N. Rowley, *Phys. Rev. C* **52**, 3151 (1995).
- [10] T. Rajbongshi and K. Kalita, *Cent. Eur. J. Phys.* **12**, 433 (2014).
- [11] C. E. Aguiar, V. C. Barbosa, L. F. Canto, and R. Donangelo, *Phys. Lett. B* **201**, 22 (1988).
- [12] C. E. Aguiar, V. C. Barbosa, L. F. Canto, and R. Donangelo, *Nucl. Phys. A* **472**, 571 (1987).
- [13] C. E. Aguiar, V. C. Barbosa, L. F. Canto, and R. Donangelo, *Nucl. Phys. A* **500**, 195 (1989).
- [14] S. Gil and D. E. DiGregorio, *Phys. Rev. C* **57**, R2826 (1998).
- [15] R. C. Lemmon *et al.*, *Phys. Lett. B* **316**, 32 (1993).
- [16] J. R. Leigh, J. J. M. Bokhorst, D. J. Hinde, and J. O. Newton, *J. Phys. G* **14**, L55 (1988).
- [17] M. J. Rhoades-Brown and V. E. Oberacker, *Phys. Rev. Lett.* **50**, 1435 (1983).
- [18] L. T. Baby, V. Tripathi, J. J. Das, P. Sugathan, N. Madhavan, A. K. Sinha, M. C. Radhakrishna, P. V. Madhusudhana Rao, S. K. Hui, and K. Hagino, *Phys. Rev. C* **62**, 014603 (2000).
- [19] H. Timmers *et al.*, *Nucl. Phys. A* **633**, 421 (1998).
- [20] H. M. Jia, C. J. Lin, F. Yang, X. X. Xu, H. Q. Zhang, Z. H. Liu, Z. D. Wu, L. Yang, N. R. Ma, P. F. Bao, and L. J. Sun, *Phys. Rev. C* **90**, 031601(R) (2014).
- [21] A. K. Sinha *et al.*, *Nucl. Instrum. Methods A* **339**, 543 (1994).
- [22] E. T. Subramaniam, B. P. Ajith Kumar, and R. K. Bhowmik, CANDLE – Collection and Analysis of Nuclear Data using Linux nEtnetwork (unpublished).
- [23] R. Brun and F. Rademakers, ROOT – An Object Oriented Data Analysis Framework, Proceedings of the AIHENP96 Workshop, Lausanne, September 1996 [*Nucl. Instrum. Methods A* **389**, 81 (1997)]. See also <http://root.cern.ch/>
- [24] S. Nath, P. V. Madhusudhana Rao, S. Pal, J. Gehlot, E. Prasad, G. Mohanto, S. Kalkal, J. Sadhukhan, P. D. Shidling, K. S. Golda, A. Jhingan, N. Madhavan, S. Muralithar, and A. K. Sinha, *Phys. Rev. C* **81**, 064601 (2010).
- [25] S. Nath, *Comput. Phys. Commun.* **180**, 2392 (2009).
- [26] A. Gavron, *Phys. Rev. C* **21**, 230 (1980).
- [27] T. Banerjee, S. Nath, and S. Pal, *Phys. Rev. C* **91**, 034619 (2015).
- [28] T. Sikkeland, *Phys. Rev.* **135**, B669 (1964).
- [29] K. Hagino, N. Rowley, and A. T. Kruppa, *Comput. Phys. Commun.* **123**, 143 (1999).
- [30] S. Raman, C. W. Nestor, Jr., and P. Tikkanen, *At. Data Nucl. Data Tables* **78**, 1 (2001).
- [31] D. L. Hendrie, *Phys. Rev. Lett.* **31**, 478 (1973).
- [32] R. H. Spear, *At. Data Nucl. Data Tables* **42**, 55 (1989).
- [33] O. Akyüz and A. Winther, in *Nuclear Structure and Heavy-ion Reactions*, edited by R. A. Broglia *et al.*, Proceedings of the International School of Physics Enrico Fermi Course LXXVII, Varenna (North-Holland, Amsterdam, 1981).
- [34] B. S. Nara Singh, V. Nanal, and R. G. Pillay, *Pramana J. Phys.* **61**, 507 (2003).
- [35] D. L. Hendrie *et al.*, *Phys. Lett. B* **26**, 127 (1968).
- [36] H. J. Wollersheim, W. Wilcke, and T. W. Elze, *Phys. Rev. C* **11**, 2008 (1975).
- [37] P. Möller, *Nucl. Phys. A* **142**, 1 (1970).
- [38] U. Götz, H. C. Pauli, K. Alder, and K. Junker, *Nucl. Phys. A* **192**, 1 (1972).
- [39] P. Möller *et al.*, *Phys. Lett. B* **26**, 418 (1968).
- [40] S. G. Nilsson *et al.*, *Nucl. Phys. A* **131**, 1 (1969).
- [41] T. Cooper *et al.*, *Phys. Rev. C* **13**, 1083 (1976).
- [42] P. Möller, J. R. Nix, W. D. Myers, and W. J. Swiatecki, *At. Data Nucl. Data Tables* **59**, 185 (1995).
- [43] A. A. Aponick, Jr., C. M. Chesterfield, D. A. Bromley, and N. K. Glendenning, *Nucl. Phys. A* **159**, 367 (1970).